DOI: https://doi.org/10.54966/7h6r0c17

Journal of Renewable Energies

Revue des Energies Renouvelables

Journal home page: https://revue.cder.dz/index.php/rer

Research paper

Electromagnetic shielding properties of polymer blended with graphene sheets and iron oxide particles

Mourad Makhlouf [a,b,*], **Sabrina Bouriche** [b], **Zoubir Benmaamar** [b], **Didier Villemin** [c]

[a] *Scientific and Technological Research Directorate - Cherchell Academy DPHB, Tipaza, Algeria*

[b] *Laboratory of Energy Processes and Nanotechnology -University of Blida-Algeria*

[c] *Laboratory of Molecular and Thio-organic Chemistry, UMR CNRS 6507, INC3M, FR 3038, ENSICAEN and Research Center, University of Caen, France*

ARTICLE INFO

Article history:
Received December 20, 2024
Accepted May 29, 2025
Available online June 5, 2025
Published June 26, 2025

Keywords:
Graphene (G),
Fe2O3 nanoparticles,
Nanocomposites,
Electromagnetic interference (EMI),
Shielding efficiency (SE).

ABSTRACT

This work introduces an innovative polymer composite for electromagnetic interference (EMI) shielding, combining recycled graphene sheets and iron oxide (Fe2O3) particles within a PVC matrix. The goal was to develop a lightweight and effective material to attenuate electromagnetic disturbances, particularly in the band frequency range (10-15 GHz). An ultra-thin (2 mm) composite containing only 10% recycled graphene, obtained from spent batteries, achieved electromagnetic shielding effectiveness (SE) of 38.5 dB in this frequency band. This result demonstrates a significant synergy between graphene and Fe2O3, where the addition of Fe2O3 enhanced graphene dispersion via ligand exchange, thereby lowering the percolation threshold and increasing wave absorption. These key findings highlight the potential of this composite for EMI shielding applications in high-stress environments. Future research perspectives include optimizing the graphene/Fe2O3 composition to further enhance shielding effectiveness, exploring the impact of different Fe2O3 morphologies, and evaluating the environmental stability and durability of the composite under various operational conditions. Furthermore, investigating the integration of this composite into specific electronic devices, such as 5G communication systems and wearable devices, will validate its practical application and commercial potential.

1. INTRODUCTION

The rise of electronic devices in our daily lives has led to increasing interest in the issue of electromagnetic interference (EMI) (Bayat et al., 2014; Miller et al., 2022). This phenomenon has

* *Corresponding author, E-mail address: makhlouf_mourad@univ-blida.dz*

ISSN: 1112-2242 / EISSN: 2716-8247

resulted in electromagnetic pollution, causing data loss, signal interference, system failures, and growing concerns about information and communication security, as well as human health (Wang et al., 2019; Rajavel et al., 2020; Mazzoli et al., 2018).

Technological advancements have made human exposure to electromagnetic fields practically unavoidable, highlighting the need for a comprehensive understanding (Wan et al., 2020; Arjmand et al., 2012).

The distinctive characteristics of electromagnetic waves remain significantly influential, posing a notable challenge (Mueller et al., 1988). Their effects manifest in various outcomes, including alterations in physiological markers, genetic effects, and overall health. The increasing prevalence of harmful electromagnetic waves necessitates heightened vigilance to mitigate them (Liu et al., 2007; Kunkel et al., 2019). Additionally, the ability of electromagnetic waves to penetrate shielding materials at higher frequencies is a crucial factor to consider (Al-Gharram et al., 2025).

Renewable energy installations, while crucial for a sustainable future, are not without their challenges, particularly those related to electromagnetic interference (EMI) (Dincer, 2000). This interference can affect the operation of the installations themselves as well as other nearby systems, and vice versa (Williams & Amstrong, 1999). Problems with electromagnetic interference (EMI) encountered in photovoltaic solar installations (PVIs) are a growing concern due to the rapid expansion of this technology (Kane et al., 2024). These issues arise when PVIs act as sources of interference, affecting other systems (Marion & Smith, 2017). EMI emissions from PVIs can disrupt systems such as air traffic communication systems (Linder & Wiklundh, 2022), hospitals (Hut, 2019), and telephone networks (Singh et al., 2023).

Electromagnetic waves, known as electromagnetic radiation, emanate from charged particles and can pass through various media, including air, space, and matter. Metals and their composite alloys have become prominent in electromagnetic interference (EMI) shielding, where metal fillers enhance shielding effectiveness (Ortlek et al., 2012; Song et al., 2025). Metal sheets, such as copper, silver, nickel, tin, and steel, along with metal foams, are preferred due to their physical properties, such as thickness, weight, permeability, conductivity, and solderability, which affect their reflection and absorption capabilities (Ayub et al., 2021).

Previous reviews have discussed graphene and iron-reinforced polymer composites in electromagnetic interference (EMI) shielding applications, but there is still a need for deeper and more comprehensive research. Carbon-based materials, known for their exceptional conductivity and flexibility, have emerged as a leading force in the field of EMI shielding. Carbon fillers, including carbon black and carbon fibers, have played a critical role in achieving the desired shielding effectiveness (Al-Saleh et al., 2013; Rahman et al., 2023; Shetty et al., 2023).

The introduction of carbon particles and carbon nanotubes has yielded promising results (He et al., 2024). However, concerns persist regarding the limited mechanical flexibility of carbon-based materials and the corrosion and weight issues associated with metal-based counterparts (Zheng et al., 2022). Therefore, it is vital to identify a lightweight, durable, low-cost, environmentally friendly, and comprehensive shielding material, especially in light of the growing electromagnetic pollution associated with the advent of 5th generation (5G) telecommunication systems and high-frequency electronic interfaces (Huang et al., 2023; Modanwal et al., 2024).

However, our approach is distinguished by the use of recycled graphene and the introduction of Fe_2O_3 for electromagnetic shielding. This graphene exhibits several distinctive properties, including its light weight (Tiwari et al., 2020), its flexibility (Lee et al., 2015), and its excellent shielding performance (Lin et al., 2019), which makes it a suitable choice for protecting sensitive electronic components in

renewable energy systems (Kausar et al., 2023). Studies have also examined the effect of iron oxide nanoparticles on electromagnetic shielding properties (Wang et al., 2020; Kaur et al., 2012). Nevertheless, our research focuses on the specific synergy between recycled graphene and Fe_2O_3 in a PVC matrix. Studies on battery recycling and graphene extraction are also available (Fleuriault et al., 2019; Larsson et al., 2014).

2. METHODS

Polyvinyl chloride (PVC) was purchased from Aldrich (Mw = 80000 g/mol). The graphite powder (graphite rod from used batteries), dibutylsebacate (DBS), 98% H2SO4, and ferric chloride FeCl3were purchased from Aldrich, along with demineralized water.

2.1 Synthesis of Graphene G

In a conventional electrochemical process (Bouriche et al., 2022); (Bakli et al., 2022), a two-electrode configuration was utilized, with a graphite rod acting as the anode and another rod serving as the cathode within a solution of sulfuric acid (H_2SO_4). The electrolyte comprised a 100ml aqueous mixture with a volume ratio of 1:4 H_2SO_4 to H_2O. The application of a direct current (DC) voltage of 10 V resulted in the complete consumption of the graphite rod, with graphene sheets transforming within 1.5 hours. After 30 minutes, the aqueous graphene ink solution was subjected to centrifugation and multiple washes with distilled water. Subsequently, the graphene material was subjected to a 24-hour drying period at 60°C.

2.2 Grafting of iron oxide (Fe_2O_3) onto graphene (G) through a hydrothermal process

The hydrothermal method (Ma et al., 2018) was used to carry out the grafting of iron oxide (Fe_2O_3) onto graphene (G). (Tran Van et al., 2019). The process begins with the preparation of an aqueous solution of ferric chloride, specifically using 1.26 grams of $FeCl_3.6H_2O$ within 100 milliliters of water. The solution is then stirred for three and a half hours to ensure a uniform solution is achieved. Concurrently, another aqueous solution is prepared, containing 1 g of graphene (G) within 100 milliliters of water. The solution is then subjected to a 100-minute sonication process, which ensures uniform consistency. The uniform graphene solution is then introduced gradually into the first ferric chloride solution. Subsequently, a concentrated aqueous solution of sodium hydroxide (NaOH) is added meticulously, drop by drop, to the amalgamated solution. The process is accompanied by stirring to achieve a pH value of approximately 11. Once this pH level has been attained, the resulting solution undergoes vigorous stirring for a further 30 minutes. Thereafter, the solution is transferred to an autoclave and subjected to hydrothermal treatment at a temperature of 180 °C for 3 hours.

2.3 Preparation of $(PVC)_x(G\text{-}Fe)_y$ nanocomposites

The first step is to combine G/Fe_2O_3 with DBS, followed by a 15 minutes sonication period. This step is crucial for ensuring the effective dispersion of G/Fe_2O_3 and preventing its agglomeration. Subsequently, PVC is added. The resulting mixture is then poured carefully into a mold and placed in an oven for one hour and 30 minutes at a temperature of 155°C. Furthermore, to examine the influence of fillers on PVC characteristics, a series of nanocomposites is meticulously developed (Wang et al., 2020; Suma et al., 2025). The resulting compositions are outlined in Table 1 for your convenience.

3. CHARACTERIZATION TECHNIQUE

Raman spectroscopy was used to facilitate observation and characterization, enabling an analysis of the material's molecular composition and structural attributes. Our samples were subjected to detailed examination using a Renishaw spectrometer, calibrated for monochromatic laser radiation (Ar^+) at a wavelength of 514.5 nm. The X-ray diffraction (XRD) analysis provided valuable insights into the microstructure of the crystalline phases inherent in our samples. To this end, our samples were evaluated using a D8 Advance Eco diffractometer (Bruker) with a copper tube (λ = 1.54 Å). To gain further insight into the morphology and structural features of the nanocomposite samples, scanning electron microscopy (SEM) (Quanta FFG 250) was employed. In assessing the electromagnetic shielding capabilities of the (G/PVC) layers, a vector network analyzer-connected device, specifically the rectangular waveguide, proved to be a crucial instrument for measurement.

Table 1. The compositions of the various G/Fe_2O_3 composite materials.

PVC%	DBS %	G/Fe_2O_3 %
45	55	0
45	52	3
45	50	5
45	45	10

4. RESULTS AND DISCUSSION

Raman spectroscopy is an invaluable technique for discerning the characteristics of both sp^2 and sp^3 hybrid carbon atoms. It is particularly effective at elucidating the features of various carbon structures, including graphite (Fig. 1.a) and graphene (Fig. 1.b). Furthermore, the ability to distinguish between single, double, and multilayer graphene is confirmed through unique Raman patterns.

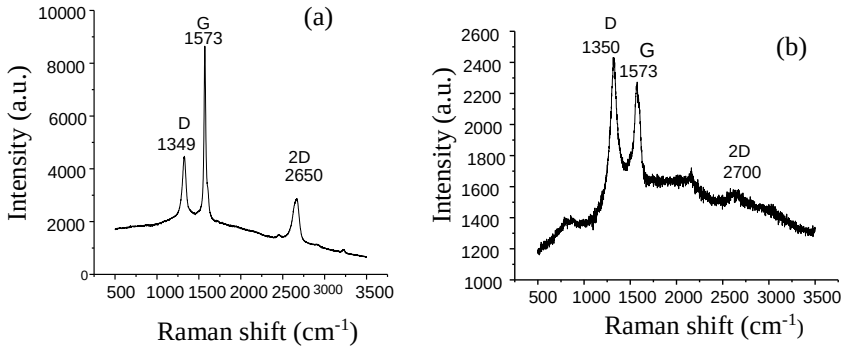

Fig 1. Raman spectra of graphite (a) and graphene (b).

The I_D/I_G ratio, which has traditionally been used to indicate inter-defect distance in graphene, has been found to have limitations when applied to graphene oxide (GO) (Kaushal et al., 2019; Chauhan et al., 2023). Chhowalla and Ferrari proposed a new amorphization trajectory, whereby the I_D/I_G ratio of carbon (sp^2) increases in line with the expansion of defects. This is linked to the square of the crystallite size (Chhowalla et al., 2000). Beaulieu et al. (2014) state that an increase in the defect intensity ratio (I_D/I_G) is indicative of an augmentation in the number of defects. A reduction in the ratio of D and G bands' intensities (I_D/I_G ratio) (Table 2), coupled with a shift towards lower wavenumbers (cm^{-1}), indicates a contraction in the extent of graphitic domains. This contraction is attributed to an increase in

disorder in SP^2 bonds and a corresponding increase in SP^3 bonds within the structure. A lower I_D/I_G ratio (resembling graphite) is indicative of an intensified density of defects (Lucchese et al., 2010).

Table 2. Summary of the D and G band intensities, represented as the I_D/I_G ratio.

Sample	D -Intensity (u.a)	G -Intensity (u.a)	I_D/I_G
Graphite	4411	8565	0.52
G	2427	2260	1.07

Furthermore, the X-ray spectrum of the graphite powder (Fig. 2.a) displays a hexagonal structure consistent with the (002) orientation. This is indicated by a single peak at $2\theta = 26°$, which corresponds to an approximate spacing of 3.4 Å between the graphite planes.

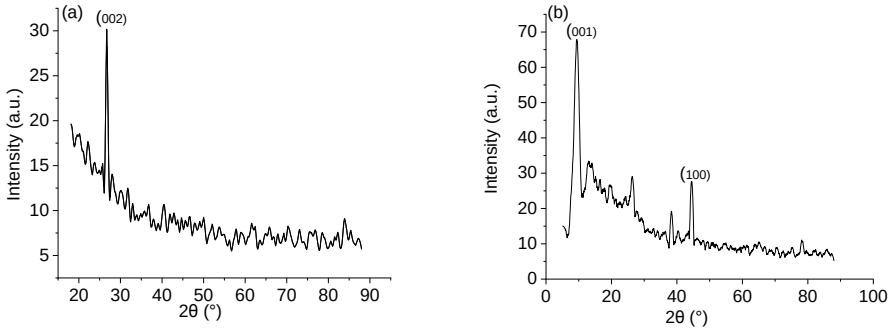

Fig 2. XRD patterns of Graphite (a) and Graphene (b)

Fig. 2.b illustrates the X-ray spectra of graphene (G), which displays a notable absence of the diffraction peak in comparison to the graphite pattern ($2\theta = 26.4°$). This absence indicates the elimination of structural periodicity in exfoliated graphene. It is clear that the increased inter-layer spacing resulting from graphite oxidation is caused by the introduction of oxygen-containing groups between the graphite layers. This process reduces the van der Waals forces binding the layers, making them easier to separate through sonication in an aqueous medium.

Fig. 3.a illustrates the examination via scanning electron microscope (SEM), which showcases the amplification of graphite grains. This SEM image demonstrates a more uniform expansion within the milled sample. Further insight can be gleaned from Fig. 3.b, which shows our products' images vividly illustrating the dynamic configuration of graphene, confirming the presence of structural uniformity on a microscopic scale. The images portray extensive and intact graphene sheets (G) intertwined atop each other, a phenomenon that is more pronounced under higher magnification.

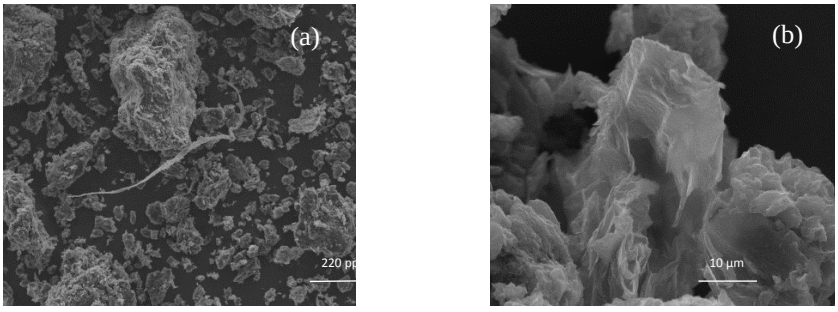

Fig 3. SEM of Graphite (a) and Graphene (b)

The FTIR spectra obtained for G, Fe_2O_3 and G/Fe_2O_3 are shown in Figure 4.

Moreover, the spectrum of G shows characteristic peaks of G from the literature, namely absorption bands at 1630 and 1530 cm^{-1}. This is attributed to C=O and C=C vibrations, respectively. The signal intensity located at 3500-3700 cm^{-1} due to the vibration of hydroxyl groups and water molecules, the peak at 1020 cm^{-1} due to bending vibration of C-OH and the peak at about 650 cm^{-1} representing ≡ C-H - groups. The spectrum of Fe_2O_3 shows bands that are the spectral signature of surface water (O-H stretching vibration near 3400 cm^{-1} and H-O-H bending vibration near 1625 cm^{-1}) and CO_2 from the air whose spectrum is near 2440 cm^{-1}. A strong absorption band (~560 cm^{-1}) exhibits the Fe–O bonding spectral signature, the only peak characteristic of hematite particles (Yun et al.,2014; Dong et al., 2010; Xu et al., 2011).

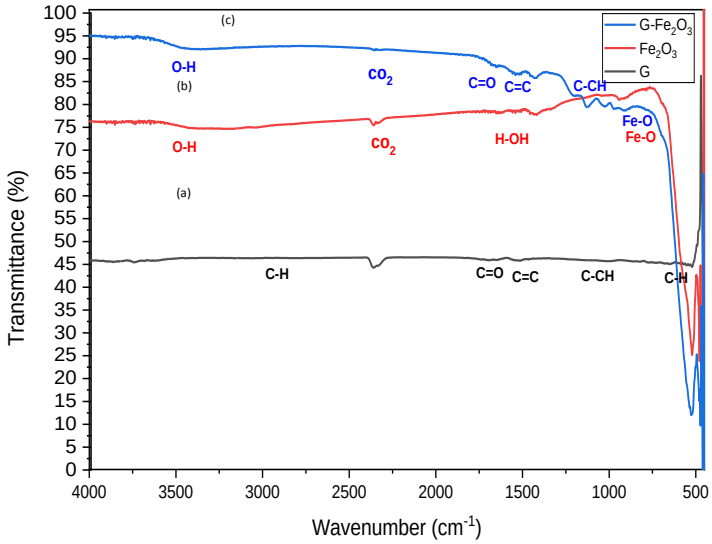

Fig 4. FTIR spectra: (a) G, (b) Fe_2O_3, (c) G-Fe_2O_3.

Furthermore, the superposition of the spectra of the G/Fe_2O_3 nanocomposite shows the band (2440 cm^{-1}). Corresponding to atmospheric CO_2, which is the two characteristic peaks of Fe_2O_3, the same absorption bands at 1630 and 1530 cm^{-1} for C=O and C=C, respectively, confirming the grafting stage (Shulga et al.,2010). To confirm the results obtained with FTIR, a complementary analysis was performed with Raman and the results obtained are shown in Figure 5.

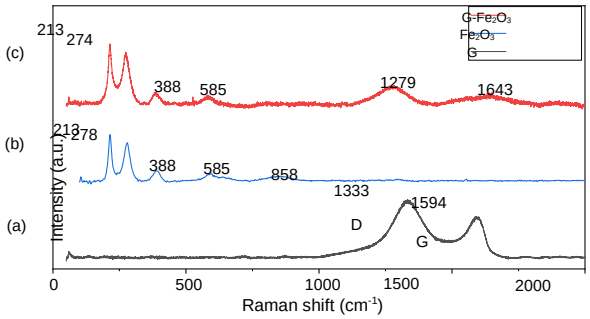

Fig 5. Raman spectra: (a) G、(b) Fe_2O_3、(c) G-Fe_2O_3.

Figure 6 illustrates the scanning electron microscopy of G-Fe_2O_3 nanoparticles. However, as shown in this figure, numerous spherical-shaped Fe_2O_3 nanoparticles at the nanoscale are observed, much better

dispersed on the graphene sheets. This suggests that graphene can reduce the agglomeration of Fe_2O_3 nanoparticles.

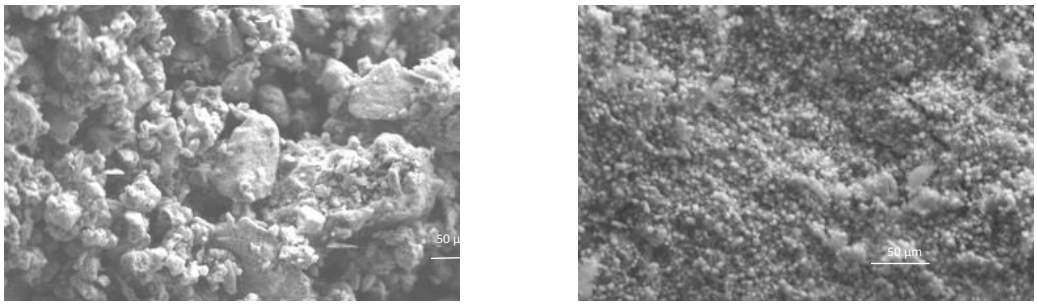

Fig 6. SEM de G-Fe_2O_3

5. EMI SHIELDING

EMI shielding materials are of great importance in the context of modern computer and telecommunications technologies (Rubežienė et al., 2020). (Bhattacharjee et al., 2020). These materials are used in a wide range of applications, including commercial and scientific electronic devices, antenna systems, and military electronics (Gadhafi et al., 2016). (García et al., 2024). In recent years, there has been a notable shift in focus towards the advancement of EMI shielding materials (Lu et al., 2024). The hybrid materials discussed earlier, comprising graphene, magnetic nanocrystals, and polymers, demonstrate a range of multifunctional attributes, including superparamagnetic behavior (Li et al., 2024). The combination of electrical and magnetic properties in materials is particularly attractive for use in electromagnetic devices (Lee et al., 2014).

EMI shielding values for various composite materials, including multifunctional carbon materials with Fe components, are detailed in Table 3.

Table 3. EMI shielding values of different composite materials

Materials	Thickness/ mm	SE/dB	Frequency/ GHz	Ref.
α-Fe_2O_3 nanoflake	5	−41.67	2.8	(Yang et al ., 2019)
Urchin like α-Fe_2O_3	1–5	−9.2	3.76–8.15	(Tong., 2011)
γ-Fe_2O_3 dendritic	4	-50	2–13	(Sun et al .,2011)
γ-Fe_2O_3 nanosphere	3	-18	14.8	(Wu et al .,2015)
Porous α-Fe_2O_3 nanosphere	2	-60	16.6	(Lv et al.,2015)
HCNT/Fe@Fe_2O_3	4	38.2	5	(Chen et al., 2019)
$ZnFe_2O_4$@graphene/TiO_2	2.5	55.5	3.8	(Wang et al., 2017)
Graphene@Fe_3O_4@WO_3@PANI	4	46.7	9.4	(Wang et al., 2017)
$NiFe_2O_4$ nanorod/graphene	2	-29.2	16.1	(Fu et al., 2013)
α-Fe_2O_3 nanorod/graphene	2	-45	12.8	(Wang et al., 2018)
Fe_3O_4//graphene	1.5	-29	8-12	(Song et al., 2015)
$ZnFe_2O_4$@graphene@TiO_2	2.5	-55.6	3.8	(Wang et al., 2017)
Cu/ graphene/epoxy	2	47	8.2–12.4	(Yanget al., 2019)

Table 3 provides an overview of the EMI shielding performance of various composite materials, highlighting the influence of composition, morphology, thickness, and frequency. It presents a wide diversity of composite materials, allowing for comparison of their shielding performance. It is observed that the morphology of Fe_2O_3 has a significant impact on shielding performance. The addition of graphene generally improves shielding performance, as seen in several composites. Shielding performance varies with frequency. Some materials are more effective at specific frequencies.

This study aims to demonstrate the potential of these multifunctional hybrid composites as candidates for electromagnetic interference (EMI) shielding materials. In this study, we evaluated the electromagnetic shielding effectiveness (EMI SE) of samples measuring 2 mm in thickness across the frequency range of 10 to 15 GHz.

Figure 7 shows the EMI shielding curves of PVC/G/Fe_2O_3 composites. As an insulator, unadulterated PVC exhibits nearly negligible EMI shielding effectiveness within the (10–15 GHz) frequency band.

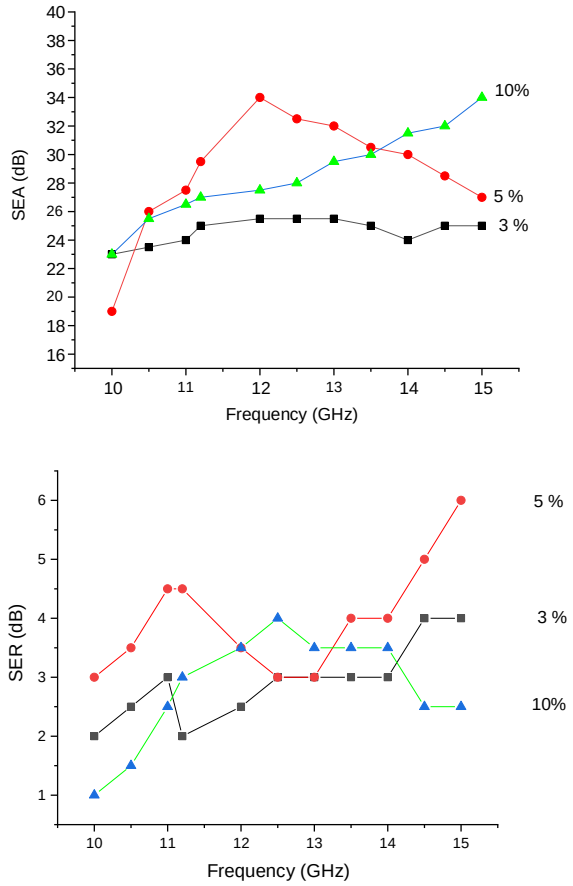

Fig 7. EMI shielding efficiency as a function of frequency measured in the 8-15 GHz range of PVC/ G/Fe_2O_3

The SEA and SER values present the shielding effectiveness obtained for PVC/graphene/Fe_2O_3 composites at different loadings in the band (10-15 GHz). According to classical electromagnetic wave theory (Ott et al., 2009) , the total shielding effectiveness (SET) of a composite is expressed in terms of the ratio of the incident power on the composite surface and the transmitted power , and can be mathematically expressed in logarithmic scale, in dB as SE=SET=SER+SEA+SEM (Al-Ghamdi et al., 2016; Bouriche al., 2022). where SER and SEA represents the contributions in total shielding effectiveness due to reflection and absorption, respectively, SEM represents the additional effects of

multiple reflections and transmissions (Paul et al., 2006) and can be neglected (Al-Ghamdi et al.,2010) in all practical application .

Table 4 presents the Electromagnetic Interference (EMI) Shielding Effectiveness (SE) in decibels (dB) for PVC/graphene/Fe_2O_3 composite materials with varying weight percentages of the filler (3%, 5%, and 10%). The results are shown across three different frequency bands: 0-10 GHz, 10-12 GHz, and 12-15 GHz.

Table 4. EMI Shielding Effectiveness obtained for the PVC/graphene/Fe_2O_3 composites

Frequency Bands	SEA (dB)			SER (dB)			Max SE (dB)		
	3 %	5%	10 %	3 %	5 %	10 %	3 %	5 %	10 %
0-10 GHz	23	19	23	2	3	3.75	25	22	26.75
10-12 GHz	25	34	27	2.75	4.5	6	27.75	38.5	33
12-15 GHz	23	28	34	3.75	3.5	4.25	26.75	31.5	38.25

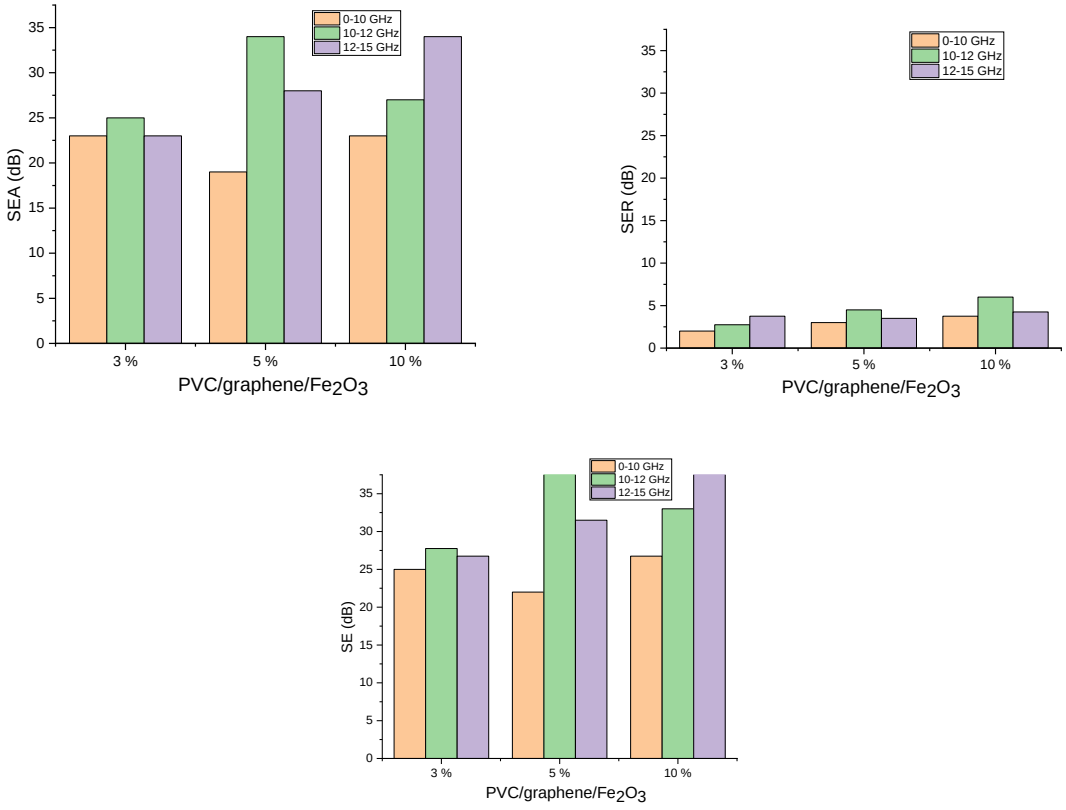

Fig 8. Column of EMI shielding efficiency as a function of frequency in the 8-15 GHz range

According to the table 4 and Figure 8, the maximum SE value increases significantly with filler content, from 3% to 5%, reaching 38.5 dB. However, a further increase in filler content to 10% results in a slight decrease in the maximum total SE, to 38.25 dB. The significant increase in the maximum SE from 3% to 5% filler content is likely due to a substantial improvement in the conductivity and permeability of the composite. The slight decrease in the maximum SE when increasing to 10% filler content could be attributed to phenomena such as the saturation of the filler's effect, particle aggregation, or complex effects related to increased interfacial reflections. This observed behavior is a result of the competition between the improvement of electromagnetic properties due to the increase in filler concentration and

the negative effects that appear at higher concentrations, such as saturation and particle aggregation. The optimal point (here, 5% filler content) represents a compromise where the benefits of adding filler are maximized before the drawbacks of the high concentration become predominant.

As illustrated in Table 5, several solutions have been devised to address EMI shielding, to achieve an optimal balance between performance, cost, and applicability.

Table 5. Graphene/Fe_2O_3 and their shielding performance.

Filler Composition	Filler Loading (wt%)	Frequency Range (GHz)	Max EMI SE (dB)	Reference
Graphene oxide/Fe_2O_3	/	8.2 - 12.4	37.45	(Chen et al., 2021).
Graphene/Fe_2O_3	4 %	0.1 GHz–13.6 GHz	95.57	(Ahmad et al., 2023).
Graphene/Fe_2O_3	/	8.7 GHz	37.95	(Guo et al.,2020).
Graphene/α-Fe_2O_3	16.7 %	14.4 GHz	50.06	(Zhang et al.,2018)
Graphene/Fe_2O_3	/	7 GHz	64.3	(Chen et al.,2021)
Graphene/Fe_2O_3	3 %	10-15	28.75	This work
	5 %		40	
	10 %		38.25	

Table 5 presents a comprehensive overview of the electromagnetic interference (EMI) shielding performance of various graphene/Fe_2O_3 materials. According to this table, graphene/Fe_2O_3 composites are promising materials for shielding applications across different frequency ranges. This optimal performance results from the synergistic effects of conductive graphene and magnetic Fe_2O_3, contributing to both the reflection and absorption of electromagnetic waves.

The results of our work, applied to a slightly higher frequency range (10-15 GHz), are also presented in the table. Our data highlights the EMI shielding performance of the G-Fe_2O_3/PVC composite at different filler ratios (3%, 5%, and 10%), demonstrating that shielding effectiveness generally increases with an increase in the filler ratio within this specific composite system and frequency range.

6. CONCLUSION

The results of this study demonstrate the growing significance of composite materials in providing electromagnetic interference (EMI) protection for modern electronic applications. The production of multifunctional PVC composites involved the incorporation of graphene and Fe_2O_3 nanoparticles within the PVC matrix. The dispersion of graphene within PVC was notably enhanced through the integration of Fe_2O_3 nanoparticles, leveraging ligand exchange. This strategic approach proved highly effective, with the well-dispersed nanofillers contributing to the outstanding performance of the ternary composites. These composites demonstrated their capability to efficiently attenuate electromagnetic disturbances with exceptional electromagnetic shielding effectiveness (38.5 dB) observed in the band

frequency range (10-15 GHz). Furthermore, it is expected that further optimization of the composition between graphene and Fe2O3 nanoparticles could result in significant enhancements in the efficacy of electromagnetic shielding.

REFERENCES

Abdelal, N., Dib, N., Young, D., &Slanker, A. (2022). Electromagnetic interference shielding and dielectric properties of graphene nanoplatelets/epoxy composites in the x-band frequency range. Journal of Materials Science, 57(29), 13928–13944.

Ahmad, A. Fahad., Ab Aziz, S., Abbas, Z., Obaiys, S. J., Khamis, A. M., Hussain, I. R., & Zaid, M. H. M. (2018). Preparation of a chemically reduced graphene oxide reinforced epoxy resin polymer as a composite for electromagnetic interference shielding and microwave-absorbing applications. Polymers, 10(11), 1180.

Ahmad, H. S., Hussain, T., Nawab, Y., & Awais, H. (2023). Graphene and Fe2O3 filled composites for mitigation of electromagnetic pollution and protection of electronic appliances. Composites Science and Technology, 240, 110097. https://doi.org/10.1016/j.compscitech.2023.110097.

Al-Ghamdi, A. A., Al-Hartomy, O. A., Al-Solamy, F. R., Dishovsky, N. T., Malinova, P., Atanasov, N. T., & Atanasova, G. L. (2016). Correlation between electrical conductivity and microwave shielding effectiveness of natural rubber-based composites, containing different hybrid fillers obtained by impregnation technology. Materials Sciences and Applications, 07(09), 496–509. https://doi.org/10.4236/msa.2016.79043.

Al-Ghamdi, A.A. & El-Tantawy, F. (2010). New electromagnetic wave shielding effectiveness at microwave frequency of polyvinyl chloride reinforced Graphite/Copper nanoparticles. Composites. Part A: Applied Science and Manufacturing, 41, 1693-1701. http://dx.doi.org/10.1016/j.compositesa.2010.08.006.

Al-Gharram, M. & AlZoubi, T. (2025). Exploring dual optical responses of polyaniline-fe_2o_3 nanocomposites for advanced optoelectronic and supercapacitor applications. Ceramics International. https://doi.org/10.1016/j.ceramint.2025.03.173.

Al-Saleh, M. H., Saadeh, W. H., & Sundararaj, U. (2013). EMI shielding effectiveness of carbon based nanostructured polymeric materials: A comparative study. Carbon, 60, 146–156.

Arjmand, M., Apperley, T., Okoniewski, M., & Sundararaj, U. (2012). Comparative study of electromagnetic interference shielding properties of injection molded versus compression molded multi-walled carbon nanotube/polystyrene composites. Carbon, 50(14), 5126–5134. https://doi.org/10.1016/j.carbon.2012.06.053.

Ayub, S., Guan, B. H., Ahmad, F., &Nisa, Z. U. (2021). A shear mixing approach in polymer composite formation. 2021 Third International Sustainability and Resilience Conference: Climate Change, 205–210. doi: 10.1109/IEEECONF53624.2021.9668079.

Bakli, H., Moualhi, M., & Makhlouf, M. (2022). High-sensitivity electrical properties measurement of graphene-based composites using interferometric near-field microwave technique. Measurement Science and Technology, 33(4), 045012.

Bayat, M., Yang, H., Ko, F. K., Michelson, D., &Mei, A. (2014). Electromagnetic interference shielding effectiveness of hybrid multifunctional Fe3O4/carbon nanofiber composite. Polymer, 55(3), 936–943.

Beaulieu, E. (2014). From voter ID to party ID: How political parties affect perceptions of election fraud in the U.S. Electoral Studies, 35, 24–32. https://doi.org/10.1016/j.electstud.2014.03.003.

Bhattacharjee, Y., Biswas, S., & Bose, S. (2020). Thermoplastic polymer composites for EMI shielding applications. Materials for Potential EMI Shielding Applications, 73–99.

Bouriche, S., Makhlouf, M., Kadari, M., Bakli, H., Hamoumi, Y., Benaicha, B., Taibi, A., &Benmaamar, Z. (2022). Smart membrane absorbing electromagnetic waves based on polyvinyl chloride/graphene composites. Materials Research Express, 9(4), 045703.

Chauhan, D. S. (2023). Chapter 7 Graphene (Gr)/graphene oxide (GO) and functionalized Gr/GO in corrosion prevention. Corrosion Prevention Nanoscience, 99–120. DOI:10.1515/9783111071756-007.

Chen, C., Bao, S., Zhang, B., Chen, Y., Chen, W., & Wang, C. (2019). Coupling Fe@Fe3O4 nanoparticles with multiple-walled carbon nanotubes with width band electromagnetic absorption performance. Applied Surface Science, 467–468, 836–843.

Chen, K.-Y., Gupta, S., & Tai, N.-H. (2021). Reduced graphene oxide/Fe2O3 hollow microspheres coated sponges for flexible electromagnetic interference shielding composites. Composites Communications, 23, 100572. https://doi.org/10.1016/j.coco.2020.100572.

Chen, P., Zhang, N., Chen, W., & Wang, Y. (2021). Rhombic Fe2O3 lumps doping hollow ZnFe2O4 spheres through oxidative decomposition process implanted into graphene conductive network with superior electromagnetic wave absorption properties. Ceramics International, 47(5), 6453–6462. https://doi.org/10.1016/j.ceramint.2020.10.228.

Chhowalla, M., Ferrari, A. C., Robertson, J., &Amaratunga, G. A. J. (2000). Evolution of sp^2 bonding with deposition temperature in tetrahedral amorphous carbon studied by Raman spectroscopy. Applied Physics Letters, 76(11), 1419–1421.

Dincer, I. (2000). Renewable energy and sustainable development: a crucial review. Renewable and Sustainable Energy Reviews, 4(2), 157–175. https://doi.org/10.1016/s1364-0321(99)00011-8.

Dong, Q., Kumada, N., Yonesaki, Y., Takei, T., Kinomura, N., & Wang, D. (2010). Template-free hydrothermal synthesis of hollow hematite microspheres. Journal of Materials Science, 45(20), 5685–5691.

Fleuriault, C., Guan, X., & Grogan, J. (2019). Extraction and Recycling of Battery Materials. JOM, 71(12), 4445–4446. https://doi.org/10.1007/s11837-019-03888-9.

Fu, M., Jiao, Q., & Zhao, Y. (2013). Preparation of NiFe2O4 nanorod–graphene composites via an ionic liquid assisted one-step hydrothermal approach and their microwave absorbing properties. Journal of Materials Chemistry A, 1(18), 5577.

Gadhafi, R., &Sanduleanu, M. (2016). A modified square patch antenna with improved bandwidth performance for WiFi applications. 2016 5th International Conference on Electronic Devices, Systems and Applications (ICEDSA), 1–4.

García, E., Andújar, A., &Anguera, J. (2024). Overview of reconfigurable antenna systems for IoT devices. Electronics, 13(20), 3988.

Guo, J., Zhan, R., & Qiu, J. (2020). Electromagnetic wave absorbing performances with Fe2O3 nanotubes/reduced graphene oxide composite sponge. Journal of Materials Science: Materials in Electronics, 31(14), 11366–11378. https://doi.org/10.1007/s10854-020-03685-0.

He, Z., &Gu, S. (2024). Sustainable development of a low-carbon supply chain economy based on the internet of things and environmental responsibility. International Journal of Sustainable Development, 1(1).

Huang, C., & Dong, Y. (2023). Multifunctional composite foam with high strength and sound-absorbing based on step assembly strategy for high performance electromagnetic shielding. Polymer Composites, 44(8), 4993–5002. https://doi.org/10.1002/pc.27465.

Hut, E. (2019). EMC-Aspecten van PV-Installaties. Agentschap Telecom. EMC Aspects of PV Installation. Available online: https://fhi.nl/app/uploads/sites/42/2019/11/Agentschap-Telecom.

Jiang, Q., Liao, X., Li, J., Chen, J., Wang, G., Yi, J., Yang, Q., & Li, G. (2019). Flexible thermoplastic polyurethane/reduced graphene oxide composite foams for electromagnetic interference shielding with high absorption characteristic. Composites Part A: Applied Science and Manufacturing, 123, 310–319.

Kane, M. M., Taylor, N., & Månsson, D. (2024). Electromagnetic interference from solar photovoltaic systems: A Review. Electronics, 14(1), 31. https://doi.org/10.3390/electronics14010031.

Kashi, S., Gupta, R. K., Baum, T., Kao, N., & Bhattacharya, S. N. (2016). Dielectric properties and electromagnetic interference shielding effectiveness of graphene-based biodegradable nanocomposites. Materials & Design, 109, 68–78. https://doi.org/10.1016/j.matdes.2016.07.062.

Kaur, A., Ishpal, & Dhawan, S. K. (2012). Tuning of EMI shielding properties of polypyrrole nanoparticles with surfactant concentration. Synthetic Metals, 162(15–16), 1471–1477.

Kausar, A., Ahmad, I., & Lam, T. D. (2023). Graphene footprints in energy storage systems—An overview. E-Prime - Advances in Electrical Engineering, Electronics and Energy, 6, 100361.

Kaushal, A., Dhawan, S. K., & Singh, V. (2019). Determination of crystallite size, number of graphene layers and defect density of graphene oxide (GO) and reduced graphene oxide (RGO). DAE solid state physics symposium 2018. Hisar, Haryana, India. AIP Conf. Proc. 2115, 030106. https://doi.org/10.1063/1.5112945.

Kunkel, G. M. (2019). Penetration of electromagnetic wave through shielding barrier. Shielding of Electromagnetic Waves, 13–18.

Larsson, K., & Binnemans, K. (2014). Selective extraction of metals using ionic liquids for nickel metal hydride battery recycling. Green Chem., 16(10), 4595–4603.

Lee, S. H. (2014). Electromagnetic Properties of Composite Materials for the Electrical Power Device. Journal of Nanoscience and Nanotechnology, 14(7), 5455–5458.

Lee, S.-M., Kim, J.-H., &Ahn, J.-H. (2015). Graphene as a flexible electronic material: mechanical limitations by defect formation and efforts to overcome. Materials Today, 18(6), 336–344.

Li, Z., Li, J., & Shen, X. (2024). Multifunctional magnetic graphene/nano cellulose hybrid aerogel with excellent electromagnetic wave absorption and thermal insulating performances. Diamond and Related Materials, 149, 111573.

Liang, J., Wang, Y., Huang, Y., Ma, Y., Liu, Z., Cai, J., Zhang, C., Gao, H., & Chen, Y. (2009). Electromagnetic interference shielding of graphene/epoxy composites. Carbon, 47(3), 922–925.

Lin, S., Ju, S., Zhang, J., Shi, G., He, Y., & Jiang, D. (2019). Ultrathin flexible graphene films with high thermal conductivity and excellent EMI shielding performance using large-sized graphene oxide flakes. RSC Advances, 9(3), 1419–1427.

Liu, Q., He, X., Yi, C., Sun, D., Chen, J., Wang, D., Liu, K., & Li, M. (2020). Fabrication of ultra-light nickel/graphene composite foam with 3D interpenetrating network for high-performance electromagnetic interference shielding. Composites Part B: Engineering, 182, 107614.

Liu, Z., Bai, G., Huang, Y., Ma, Y., Du, F., Li, F., Guo, T., & Chen, Y. (2007). Reflection and absorption contributions to the electromagnetic interference shielding of single-walled carbon nanotube/polyurethane composites. Carbon, 45(4), 821–827.

Lu, W., & Guan, H. (2024). Multi-functional electromagnetic interference (EMI) shielding materials. Electromagnetic Wave Absorption and Shielding Materials, 267–315.

Lucchese, M. M., Stavale, F., Ferreira, E. H. M., Vilani, C., Moutinho, M. V. O., Capaz, R. B., Achete, C. A., &Jorio, A. (2010). Quantifying ion-induced defects and Raman relaxation length in graphene. Carbon, 48(5), 1592–1597.

Lv, H., Liang, X., Cheng, Y., Zhang, H., Tang, D., Zhang, B., Ji, G., & Du, Y. (2015). Coin-like α-Fe_2O_3@$CoFe_2O_4$ Core–Shell composites with excellent electromagnetic absorption performance. ACS Applied Materials & Interfaces, 7(8), 4744–4750.

Ma, T., Xu, Y., Sun, L., Liu, X., & Zhang, J. (2018). Synthesis of graphene/α-Fe_2O_3 nanospindles by hydrothermal assembly and their lithium storage performance. Ceramics International, 44(1), 364–368.

Marion, B., & Smith, B. (2017). Photovoltaic system derived data for determining the solar resource and for modeling the performance of other photovoltaic systems. Solar Energy, 147, 349–357. https://doi.org/10.1016/j.solener.2017.03.043.

Mazzoli, A., Corinaldesi, V., Donnini, J., Di Perna, C., Micheli, D., Vricella, A., Pastore, R., Bastianelli, L., Moglie, F., & Mariani Primiani, V. (2018). Effect of graphene oxide and metallic fibers on the electromagnetic shielding effect of engineered cementitious composites. Journal of Building Engineering, 18, 33–39.

Miller, A. B. (2022). Public health implications of exposure to wireless communication electromagnetic fields. Electromagnetic Fields of Wireless Communications: Biological and Health Effects, 79–96.

Modanwal, R. P., &Kundalwal, S. I. (2024). Design and development of low-weight and high strength electromagnetic shielding nanocomposite in a microwave frequency range. Polymer Composites. Portico.

Mueller, R. S. (1988). Oblique transmission of electromagnetic waves through a magnetized ferrite slab. Radio Science, 23(2), 183–192.

Ortlek, H. G., Saracoglu, O. G., Saritas, O., &Bilgin, S. (2012). Electromagnetic shielding characteristics of woven fabrics made of hybrid yarns containing metal wire. Fibers and Polymers, 13(1), 63–67.

Ott, H.W. (2009) Electromagnetic Compatibility Engineering. John Wiley & Sons Inc., Hoboken. http://dx.doi.org/10.1002/9780470508510.

Paul, C.R. (2006) Introduction to Electromagnetic Compatibility. 2nd Edition, John Wiley & Sons, Inc., Hoboken.

Rahaman, M. (2023). Superior mechanical, electrical, dielectric, and EMI shielding properties of ethylene propylene diene monomer (EPDM) based carbon black composites. RSC Advances, 13(36), 25443–25458.

Rajavel, K., Luo, S., Wan, Y., Yu, X., Hu, Y., Zhu, P., Sun, R., & Wong, C. (2020). 2D Ti3C2Tx MXene/polyvinylidene fluoride (PVDF) nanocomposites for attenuation of electromagnetic radiation with excellent heat dissipation. Composites Part A: Applied Science and Manufacturing, 129, 105693.

Rubežienė, V., &Varnaitė-Žuravliova, S. (2020). EMI shielding textile materials. Materials for Potential EMI Shielding Applications, 357–378.

Shetty, H. D., Ashok Reddy, G. V., Ramasamy, V., Kaliprasad, C. S., Daruka Prasad, B., Yogananda, H. S., Naik, R., Prasad, V., Koyyada, G., & Anil Kumar, Y. (2023). Electrical conductivity and electromagnetic interference shielding effectiveness of elastomer composites: Comparative study with various filler systems. Inorganic Chemistry Communications, 151, 110578.

Shulga, Y. M., Martynenko, V. M., Muradyan, V. E., Baskakov, S. A., Smirnov, V. A., & Gutsev, G. L. (2010). Gaseous products of thermo- and photo-reduction of graphite oxide. Chemical Physics Letters, 498(4–6), 287–291.

Singh, G., Cooke, T., Johns, J., Vega, L., Valdez, A., Bull, G. (2023). Telephone interference from solar PV switching. IEEE Open Access J. Power Energy, 10, 373–384.

Song, P., Cai, Z., Li, J., He, M., Qiu, H., Ren, F., Zhang, Y., Guo, H., & Ren, P. (2025). Construction of rGO-MXene@FeNi/epoxy composites with regular honeycomb structures for high-efficiency electromagnetic interference shielding. Journal of Materials Science & Technology, 217, 311–320.

Song, W.-L., Guan, X.-T., Fan, L.-Z., Cao, W.-Q., Zhao, Q.-L., Wang, C.-Y., & Cao, M.-S. (2015). Tuning broadband microwave absorption via highly conductive Fe3O4/graphene heterostructural nanofillers. Materials Research Bulletin, 72, 316–323.

Suma, J. G., Patil, Y. N., Megalamani, M. B., Rajappa, S. K., &Nandibewoor, S. T. (2025). Sensitive electrochemical analysis of uricosuric drug sulfinpyrazone using a graphene-based sensor: A first voltammetric approach. Next Materials, 7, 100346.

Sun, G., Dong, B., Cao, M., Wei, B., & Hu, C. (2011). Hierarchical Dendrite-Like Magnetic Materials of Fe_3O_4, γ-Fe_2O_3, and Fe with High Performance of Microwave Absorption. Chemistry of Materials, 23(6), 1587–1593.

Tiwari, S. K., Sahoo, S., Wang, N., &Huczko, A. (2020). Graphene research and their outputs: Status and prospect. Journal of Science: Advanced Materials and Devices, 5(1), 10–29.

Tong, G., Wu, W., Guan, J., Qian, H., Yuan, J., & Li, W. (2011). Synthesis and characterization of nanosized urchin-like α-Fe_2O3 and Fe3O4: Microwave electromagnetic and absorbing properties. Journal of Alloys and Compounds, 509(11), 4320–4326.

Tran Van, K., Nguyen Quang, V., Le Van, T., & Mai Thanh, P. (2019). Effect of temperature on the structure and properties of Fe_2O_3/graphene nanocomposites synthesized by hydrothermal method. Vietnam Journal of Science and Technology, 57(3A), 150.

Wan, Y.-J., Li, X.-M., Zhu, P.-L., Sun, R., Wong, C.-P., & Liao, W.-H. (2020). Lightweight, flexible MXene/polymer film with simultaneously excellent mechanical property and high-performance electromagnetic interference shielding. Composites Part A: Applied Science and Manufacturing, 130, 105764.

Wang, L., Bai, X., & Wang, M. (2017). Facile preparation, characterization and highly effective microwave absorption performance of porous α-Fe_2O_3 nanorod–graphene composites. Journal of Materials Science: Materials in Electronics, 29(4), 3381–3390.

Wang, L., Qiu, H., Liang, C., Song, P., Han, Y., Han, Y., Gu, J., Kong, J., Pan, D., &Guo, Z. (2019). Electromagnetic interference shielding MWCNT-Fe_3O_4@Ag/epoxy nanocomposites with satisfactory thermal conductivity and high thermal stability. Carbon, 141, 506–514.

Wang, L., Wei, X., Wang, G., Zhao, S., Cui, J., Gao, A., Zhang, G., & Yan, Y. (2020). A facile and industrially feasible one-pot approach to prepare graphene-decorated PVC particles and their application in multifunctional PVC/graphene composites with segregated structure. Composites Part B: Engineering, 185, 107775.

Wang, Q., Tang, J., Xiao, S., Wang, M., & Shi, S. Q. (2020). Natural fiber-based composites with high hydrophobic, magnetic, and EMI shielding properties via iron oxide in situ synthesis and copper film deposition. BioResources, 15(4), 8384–8402.

Wang, Y., Wu, X., Zhang, W., Luo, C., Li, J., & Wang, Q. (2017). 3D heterostructure of graphene@Fe $_3O_4$ @WO 3 @PANI: Preparation and excellent microwave absorption performance. Synthetic Metals, 231, 7–14.

Wang, Y., Zhu, H., Chen, Y., Wu, X., Zhang, W., Luo, C., & Li, J. (2017). Design of hollow $ZnFe_2O_4$ microspheres@graphene decorated with TiO 2 nanosheets as a high-performance low frequency absorber. Materials Chemistry and Physics, 202, 184–189.

Williams, T., & Armstrong, K. (1999). Interference sources, victims and coupling. EMC for Systems and Installations, 67–100. https://doi.org/10.1016/b978-075064167-8/50004-8.

Wu, H., Wu, G., & Wang, L. (2015). Peculiar porous α-Fe_2O_3, γ-Fe_2O_3 and Fe_3O_4 nanospheres: Facile synthesis and electromagnetic properties. Powder Technology, 269, 443–451.

Xu, Y., Yang, S., Zhang, G., Sun, Y., Gao, D., & Sun, Y. (2011). Uniform hematite α-Fe_2O_3 nanoparticles: Morphology, size-controlled hydrothermal synthesis and formation mechanism. Materials Letters, 65(12), 1911–1914.

Yan, D., Pang, H., Li, B., Vajtai, R., Xu, L., Ren, P., Wang, J., & Li, Z. (2014). Structured reduced graphene oxide/polymer composites for ultra-efficient electromagnetic interference shielding. Advanced Functional Materials, 25(4), 559–566. Portico.

Yang, X., Fan, S., Li, Y., Guo, Y., Li, Y., Ruan, K., Zhang, S., Zhang, J., Kong, J., &Gu, J. (2020). Synchronously improved electromagnetic interference shielding and thermal conductivity for epoxy nanocomposites by constructing 3D copper nanowires/thermally annealed graphene aerogel framework. Composites Part A: Applied Science and Manufacturing, 128, 105670.

Yang, Z., Li, M., Zhang, Y., Lyu, X., & Hu, D. (2019). Hierarchical formation mechanism of anisotropic magnetite microflakes and their superior microwave attenuation properties. Journal of Alloys and Compounds, 781, 321–329.

Yuan, Y., Jiang, W., Wang, Y., Shen, P., Li, F., Li, P., Zhao, F., & Gao, H. (2014). Hydrothermal preparation of Fe_2O_3/graphene nanocomposite and its enhanced catalytic activity on the thermal decomposition of ammonium perchlorate. Applied Surface Science, 303, 354–359.

Zhang, N., Huang, Y., & Wang, M. (2018). Synthesis of graphene/thorns-like polyaniline/α-Fe2O3@SiO2 nanocomposites for lightweight and highly efficient electromagnetic wave absorber. Journal of Colloid and Interface Science, 530, 212–222. https://doi.org/10.1016/j.jcis.2018.06.088.

Zheng, R., Yang, D., Chen, Y., Bian, Z., & Li, H. (2023). Fe2O3/TiO2/reduced graphene oxide-driven recycled visible-photocatalytic Fenton reactions to mineralize organic pollutants in a wide pH range. Journal of Environmental Sciences, 134, 11–20.